Field Strength Dependence in MRI: Advantages and Artifacts at 3T

Matt A. Bernstein Ph.D.
Associate Professor, Department of Radiology
Mayo Clinic College of Medicine
Rochester, Minnesota U.S.A.

1. Introduction

Although $B_0 = 1.5T$ remains the predominant field strength for clinical MRI, 3.0T magnets are making substantial inroads into routine practice. The move to 3.0T is driven mainly by its approximate doubling of the signal-to-noise ratio (SNR) compared to 1.5T. The improved SNR can be used to shorten the acquisition time, to improve spatial resolution at a fixed scan time, or a combination of the two. The scaling of other physical parameters such as the doubling of the susceptibility variation (as measured in hertz) can aid applications like fMRI that use the BOLD effect. Similarly the doubling of the chemical shift (again, measured in hertz) from 1.5 to 3.0T can aid peak separation for spectroscopy.

Along with its advantages, however, imaging at 3.0T presents several challenges and pitfalls. Some artifacts are more prominent on MR images acquired at 3.0T compared to 1.5T. In this abstract, several commonly observed 3.0T artifacts and their origins are described. In some cases, specific countermeasures that can be applied to reduce the artifacts are also described.

As the advantages and drawbacks of high-field imaging continue to be evaluated, successful use of 3.0T continues to be reported [1-7]. Promising applications of 3.0T include, but are not limited to, anatomical and functional neuro MR, musculoskeletal (MSK) MR, MR angiography (MRA), and cardiac MR.

To better understand the advantages of 3.0T, along with its artifacts and their origins, it is useful to recall how several physical parameters scale [8-13] as the field strength is increased from 1.5T to 3.0T. Some basic scaling relationships are reviewed in Section 2. It is important to recognize that in all of these scaling relationships, there are no abrupt changes or discontinuities in the physical parameters as the field strength is progressively increased. Therefore, any artifact that is present at 3.0T can also be present at 1.5T, although at the lower field strength the intensity of the artifact might be far less objectionable. Consequently, strictly speaking, the term "3T artifact" is a misnomer, even though it accurately describes everyday observations.

2. Scaling of physical parameters

1. *Signal-to-noise ratio (SNR).* In the range of clinically-used field strengths, $0.2T \leq B_0 \leq 3.0T$, the SNR scales approximately linearly with main field B_0:

$$SNR \propto B_0 \tag{1}$$

The linear scaling in Eq. (1) assumes that the noise in the MRI scan is originating predominantly from the patient rather than other sources, such as the electronics.

2. *Susceptibility variation.* Variations in the local B_0 field arise at boundaries between different types of tissues, such as air-soft tissue and soft tissue-bone. Although the relative frequency variation measured in parts per million (ppm) of B_0 is independent of field strength, the frequency variation measured in hertz is linearly proportional to field strength of the main magnet:

$$\Delta f \text{ [measured in Hz]} = \frac{\gamma}{2\pi} \Delta B \propto B_0 \qquad (2)$$

3. *Chemical shift* (CS). Similar to susceptibility variation, the chemical shift measured in ppm is independent of field strength, but the chemical shift measured in hertz is linearly proportional to field strength:

$$CS \text{ [measured in Hz]} \propto B_0 \qquad (3)$$

Water resonates at a Larmor frequency that is approximately 3.3-3.5 ppm higher than lipids. This corresponds to approximately 140-150 Hz per Tesla. (The range of frequencies arises because the lipid resonance is rather broad due to its multiple constituents and their relatively short T2s.) Therefore at 3.0T water resonates at a Larmor frequency approximately 420-440 Hz higher than that of fat.

4. *RF power deposition*, as measured by the specific absorption rate (SAR). In the range of clinically-used field strengths, $0.2T \leq B_0 \leq 3.0T$, SAR approximately scales quadratically with field strength:

$$SAR \propto B_0^2 \qquad (4)$$

5. *Longitudinal relaxation time (*T_1*).* The longitudinal relaxation time increases for some tissues (such as brain parenchyma) as B_0 increases, while it remains the same for others (like cerebral spinal fluid). Fortunately, the T_1 of chelated gadolinium contrast agents does not increase very much. For example, a decrease in the relaxivity R of 5-10% is typical when going from 1.5T to 3.0T. At a given concentration of contrast [Gd] (measured in units of mM), the T_1 of the tissue is given by

$$\frac{1}{T_1} = \frac{1}{T_{1_0}} + R \times [Gd], \qquad (5)$$

where T_{1_0} is the longitudinal relaxation time in the absence of contrast agents. Because the T_1 of the un-enhanced tissue typically increases more than the enhancing tissue, often equivalent doses of gadolinium chelate produce a greater effect at 3.0T than at 1.5T [7].

6. *RF wavelength (*λ*).* The RF wavelength in a medium is proportional to the speed of light in that medium c_{medium}, and inversely proportional to RF frequency f:

$$\lambda \propto \frac{c_{medium}}{f} \qquad (6)$$

The RF frequency is invariably set at (or near) the Larmor frequency, $f = (\gamma/2\pi)B_0$, with $\gamma/2\pi$ = 42.576 MHz/T. So the RF wavelength is inversely proportional to the main magnetic field B_0

$$\lambda \propto \frac{c_{medium}}{B_0} \tag{7}$$

The speed of light in the medium is equal to the speed of light in a vacuum ($c = 2.9979 \times 10^8$ m/s), reduced by a factor that depends on the electric permittivity ε and magnetic permeability μ of the medium,

$$c_{medium} = \frac{c}{\sqrt{\varepsilon\mu}} \tag{8}$$

(The permittivity and permeability in these units are both equal to unity in vacuum). Human tissue is not very magnetic, so we can assume that $\mu = 1$. Making this assumption and combining Eqs. (6) and (7) yields:

$$\lambda \propto \frac{1}{\sqrt{\varepsilon}B_0} \tag{9}$$

The dielectric constant itself usually decreases slowly with increasing frequency. For example, the dielectric constant of water for static electric fields is approximately 80, but it is only about 1.8 for electromagnetic frequencies corresponding to visible light. In the RF frequency range, the wavelength in many tissues [14] can be reduced by several fold by dielectric effects.

3. Commonly Observed 3T Artifacts

1. *Chemical shift in the frequency-encoded direction*

The chemical shift artifact in the frequency-encoded direction shifts fat relative to water [15,16] by a fixed number of pixels. At 3.0T water resonates at a Larmor frequency that is 420-440 Hz higher than that of lipids. At a fixed receiver bandwidth (BW) measured in hertz/pixel, the fat-water chemical shift will be twice as many pixels compared to 1.5T. This often leads to an objectionable amount of chemical shift in the frequency-encoded direction in 3.0T images (Fig. 1a). Fat suppression techniques can be helpful but are not applicable to all imaging protocols. A more general remedy is to double the receiver BW at 3.0T compared to corresponding 1.5T protocol (Fig. 1b). Doubling the receiver BW costs a factor of $\sqrt{2} \approx 1.4$ in the SNR. Since SNR approximately doubles when going from 1.5T to 3.0T, 3.0T still offers a remaining factor of $\sqrt{2}$ improvement in SNR, even when the chemical shift artifact is held constant.

2. *Chemical shift in the slice direction in 2D imaging*

Chemical shift in the slice direction [15] also can be objectionable at 3.0T. It is most easily observed where the fat structure is tilted relative to the slice selection direction. Figure 2a shows an example of an axial brain image, where the fat from a more cranial (superior) slice is superimposed on the image, obscuring brain tissue. Fat is shifted from anterior-to-posterior at the

front of the head, and from posterior-to-anterior at back of the head. This differs from chemical shift in the frequency-encoded direction, which (for standard Cartesian imaging) is a spatial shift in the same direction throughout the image. Reversing the sign of the slice selection gradient would alleviate this problem at the top of the head, because fat would then be shifted away from the brain, but probably would introduce the same problem at the skull base where the skull slopes in the opposite direction. A more general solution is to increase the BW of the radiofrequency (RF) pulses (Fig. 2b). This can be accomplished by reducing the duration of the RF pulses, increasing their amplitude, and increasing the amplitude of the accompanying slice selection gradients.   One disadvantage of increasing the RF bandwidth is the RF heating, because SAR is linearly proportional to RF BW. Equation (4) illustrates how SAR increases with field strength in general, so increasing the RF BW at 3.0T can be problematic for pulse sequence protocols that operate near regulatory limits. Fortunately, many pulse sequence protocols operate well below the regulatory limits for SAR at 1.5T, so that operation at 3.0T does not present a problem. Notable exceptions include some fast spin echo/turbo spin echo acquisitions (especially HASTE, i.e., single-shot methods), and TrueFISP (i.e., FIESTA or balanced FFE). Also, unlike receiver BW, RF bandwidth is typically not an operator-selectable parameter, so modification to the pulse sequence is usually required to increase it.

3. Fat/water in- and out-of-phase times for gradient echo imaging

Since the fat-water chemical shift doubles at 3.0T compared to 1.5T, the echo times TE at which fat and water are in-phase or have opposed phase are different at 3.0T. The TE times are summarized in the following table, which is based on a chemical shift of 3.4 ppm:

TE (ms)	Fat/Water in-phase	Fat/Water out-of-phase
1.5T	0, 4.6, 9.2, 13.8, …	2.3, 6.9, 11.5, …
3.0T	0, 2.3, 4.6, 6.9, …	1.2, 3.5, 5.8, …

4. Susceptibility artifacts causing incomplete inversion

A common 3.0T artifact is incomplete inversion of the magnetization in regions of rapid susceptibility variation. Many applications at both 1.5T and 3.0T use inversion pulses (e.g., FLAIR). Also, at 3.0T it is more challenging to obtain T1-weighted contrast due to longer T1 values, and a somewhat compressed spectrum of T1 values. Consequently, inversion-based pulse sequences like MP-RAGE and MDEFT are popular at 3.0T to generate T1-weighted contrast.

The incomplete inversion of magnetization often manifests as bright spots near air-tissue boundaries (Fig. 3a). An effective solution is simply to increase the RF BW of the inversion pulse (Fig. 3b). This increase in RF BW does increase SAR, but often only a single inversion pulse is used for the acquisition of multiple lines of k-space (as in MP-RAGE), in which case the SAR penalty is usually negligible.

5. Pulsatile flow artifacts

Pulsatile flow artifacts are more problematic at 3.0T for two main reasons. First, the increased SNR at 3.0T translates into increased artifact-to-noise ratio. That is, a ghost artifact that might be buried in the noise at 1.5T could be more easily visible at 3.0T. A second reason is increased susceptibility variation (measured in hertz) at 3.0T aggravates pulsatile flow artifacts [17]. Just as

at 1.5T, common solutions include gradient moment nulling (i.e., flow compensation), and ECG or peripheral triggering. With 3D acquisitions, it is also sometimes helpful to randomize the view order to spread the artifacts over two dimensions. Non-Cartesian view orders (e.g., elliptical centric or CENTRA) spread the artifacts more uniformly within the plane formed by the two phase encoding directions, which makes the artifacts less conspicuous.

6.   Central brightening (a.k.a. the "dielectric resonance") artifact

Central brightening or "dielectric resonance" artifacts [18-20] often manifest as high signal intensity in the center of the object (Fig. 4a). When the wavelength of the RF becomes comparable to the size of the object, wave effects are often observed. A quantitative analysis requires solutions to Maxwell's equations as in [20].

The wavelength of RF in air is approximately λ = 4.7 meters at 1.5T, and λ = 2.35 meters at 3.0T. This wavelength is much greater than the size of the object to be imaged, so that central brightening is not a problem when the wavelength in the medium is the same as in air. As illustrated by Eqs (6)-(9), the higher the dielectric constant of a medium, the slower the speed of light, and the shorter the wavelength becomes. The dielectric constant of human tissue can be appreciable in the RF frequency range [14], so that central brightening artifacts become more important, especially at 3.0T.

Figure 4b shows an image comparable to Fig. 4a, but acquired with an oil-based (instead of a water-based) phantom. The more uniform signal intensity and reduction in central brightening artifact is apparent with the oil-based phantom, in which the RF wavelength is much longer. Although the dielectric constant does have frequency dependence, the difference in Figs. 4a and b is expected from the static dielectric constants of water (ε = 80), and mineral oil (ε = 2). For this reason, oil-based phantoms are useful at 3.0T to measure SNR and map the true B1-sensitivity of RF coils.

We have no control over the RF wavelength in human tissue at 3.0T, so other methods must be used to reduce the central brightening artifact. These include: 1) Choosing an imaging protocol that is relatively insensitive to flip angle. 2) Using a multi-channel phased-array receive coil. Receive coils tend to have a stronger B1-sensitivity near the surface of the patient, which can partially counteract the central brightening artifact. 3) Using an image post-processing method [21] (such as *N3* [22]) that can remove low spatial frequency intensity variation in the image domain. 4) In the future, it might be possible to use advanced methods, such as crafted RF pulses, and multiple transmit channels with Transmit SENSE to equalize the RF flip angle profile [23].

Conclusion

3.0T is an increasingly popular field strength for clinical MRI. Its advantages have been well accepted for applications such as MR angiography, imaging of small structures of the MSK anatomy, and functional neuro MRI. Several imaging artifacts, however, are more prominent at 3.0T compared to 1.5T. Understanding their physical origin can help manage these artifacts through pulse sequence and image protocol design.

References

1. Uematsu H, Takahashi M, Dougherty L, Hatabu H. High field body MR imaging: preliminary experiences. Clin Imaging. 2004 May-Jun;28(3):159-62.
2. Larsson EM, Stahlberg F. 3 Tesla magnetic resonance imaging of the brain. Better morphological and functional images with higher magnetic field strength (article in Swedish). Lakartidningen. 2005 Feb 14-20;102(7):460-3.
3. Schmitt F, Grosu D, Mohr C, Purdy D, Salem K, Scott KT, Stoeckel B. 3 Tesla MRI: successful results with higher field strengths (article in German). Radiologe. 2004 Jan;44(1):31-47.
4. Lenk S, Ludescher B, Martirosan P, Schick F, Claussen CD, Schlemmer HP. 3.0 T high-resolution MR imaging of carpal ligaments and TFCC. Rofo. 2004 May;176(5):664-7.
5. Gaa J, Weidauer S, Requardt M, Kiefer B, Lanfermann H, Zanella FE. Comparison of intracranial 3D-ToF-MRA with and without parallel acquisition techniques at 1.5T and 3.0T: preliminary results. Acta Radiol. 2004 May;45(3):327-32.
6. Gibbs GF, Huston J 3rd, Bernstein MA, Riederer SJ, Brown RD Jr. Improved image quality of intracranial aneurysms: 3.0-T versus 1.5-T time-of-flight MR angiography. AJNR Am J Neuroradiol. 2004 Jan;25(1):84-7.
7. Araoz PA, Glockner JF, McGee KP, Potter DD Jr, Valeti VU, Stanley DW, Christian TF. 3 Tesla MR imaging provides improved contrast in first-pass myocardial perfusion imaging over a range of gadolinium doses. J Cardiovasc Magn Reson. 2005;7(3):559-64.
8. Jezzard P, Duewell S, Balaban RS. MR relaxation times in human brain: measurement at 4 T. Radiology 1996; 199: 773-9.
9. Kroeker RM, McVeigh ER, Hardy P, Bronskill MJ, Henkelman RM. In vivo measurements of NMR relaxation times. Magn Reson Med 1985; 2: 1-13.
10. Fischer HW, Rinck PA, Van Haverbeke Y, Muller RN. Nuclear relaxation of human brain gray and white matter: analysis of field dependence and implications for MRI, Magn Reson Med 1990; 16: 317-34.
11. Ugurbil K, Garwood M, Ellermann J, Hendrich K, Hinke R, Hu X, Kim SG, Menon R, Merkle H, Ogawa S. Imaging at high magnetic fields: initial experiences at 4T, Magn Reson Q 1993; 9: 259-77.
12. Hoult DI. Sensitivity and power deposition in a high-field imaging experiment. J. Magn. Reson. Imaging 2000; 12**:** 46–67.
13. Vaughan JT, Garwood M, Collins CM, Liu W, DelaBarre L, Adriany G, Andersen P, Merkle H, Goebel R, Smith MB Ugurbil K. 7 vs. 4 T: RF power, homogeneity, and signal-to-noise comparison in head images. Magn. Reson. Med*.* 2001; 46: 24–30.
14. Gabriel S, Corthout. The dielectric properties of biological tissues Phys.Med.Biol.1996; 41: 2231–2249.
15. Henkelman RM, Bronskill MJ. Artifacts in magnetic resonance imaging. Reviews of magnetic resonance in medicine 1987; 2: 1-126.
16. Schenck JF. The role of magnetic susceptibility in magnetic resonance imaging: MRI magnetic compatibility of the first and second kinds. Med Phys. 1996; 23: 815-50.
17. Drangova M, Pelc NJ. Artifacts and signal loss due to flow in the presence of B(o) inhomogeneity. Magn Reson Med. 1996; 35: 126-30.
18. Röschmann P. Imaging of dielectric resonance mode patterns with a 4 T whole body MR system, in: Proceedings of the Seventh SMRM, 1988, p. 267.
19. Tropp J. Image brightening in samples of high dielectric constant. Journal of Magnetic Resonance 2004; 167:12-24.
20. Collins CM, Liu W, Schreiber W, Yang QX, Smith MB. Central brightening due to constructive interference with, without, and despite dielectric resonance. J Magn Reson Imaging. 2005 Feb;21(2):192-6.
21. Arnold JB, Liow JS, Schaper KA, Stern JJ, Sled JG, Shattuck DW, Worth AJ, Cohen MS, Leahy RM, Mazziotta JC, Rottenberg DA. Qualitative and quantitative evaluation of six algorithms for correcting intensity nonuniformity effects. Neuroimage. 2001 May;13(5):931-43.
22. Sled JG, Zijdenbos AP, Evans AC A non-parametric method for automatic correction of intensity non-uniformity in MRI data. IEEE Trans Med Imaging 1998 17:87–97. http://www.bic.mni.mcgill.ca/software/N3/

23. Ullmann P, Junge S, Wick M, Seifert F, Ruhm W, Hennig J. Experimental analysis of parallel excitation using dedicated coil setups and simultaneous RF transmission on multiple channels. Magn Reson Med. 2005;54: 994-1001.

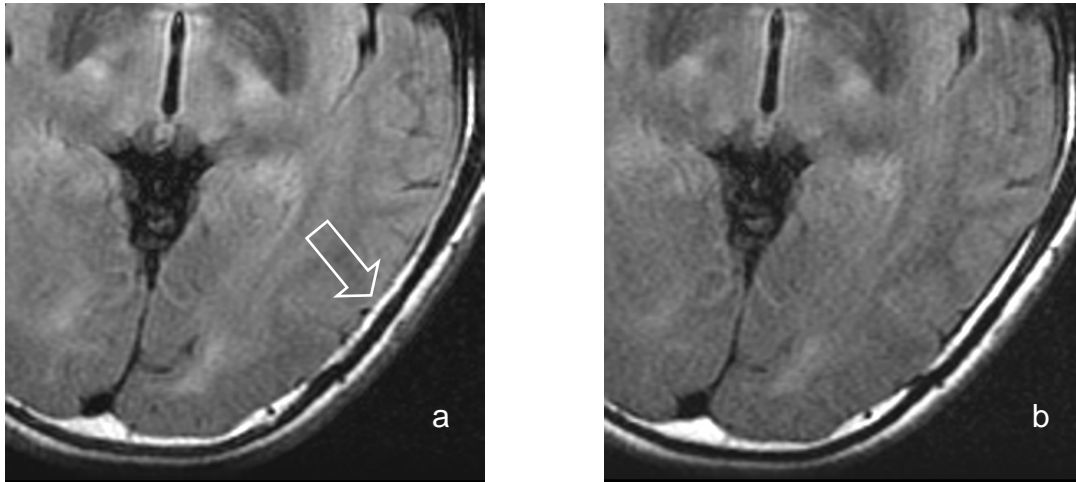Figure 1. Axial FLAIR image of a healthy volunteer at 3.0T. a) With a receiver bandwidth of 122 Hz/pixel (i.e., +/-16kHz), chemical shift in the frequency-encoded direction causes fat to overlap the brain (arrow). b) Doubling the receiver BW reduces the problem, at the cost of decreased SNR.
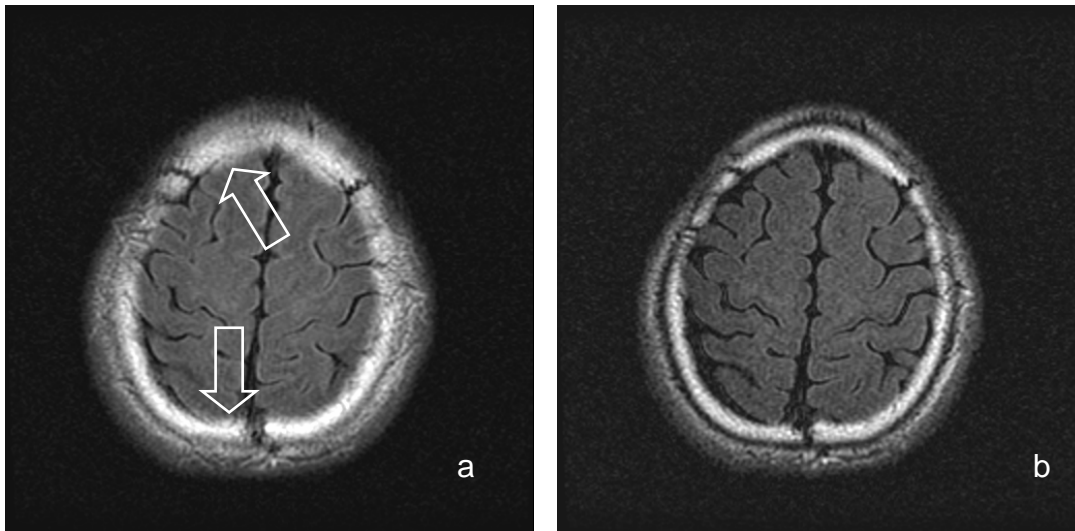
Figure 2. Axial FLAIR image of a healthy volunteer at 3.0T. a) At an excitation bandwidth of 700 Hz, chemical shift in the slice selection direction causes fat to overlap the brain (arrows). b) Doubling the excitation BW of the excitation and refocusing pulses to 1400 Hz reduces the problem, at the cost of increased SAR. (The decreased SNR in (b) is not a general problem, and occurs here because this particular pulse sequence was not optimized for higher BW RF pulses.)
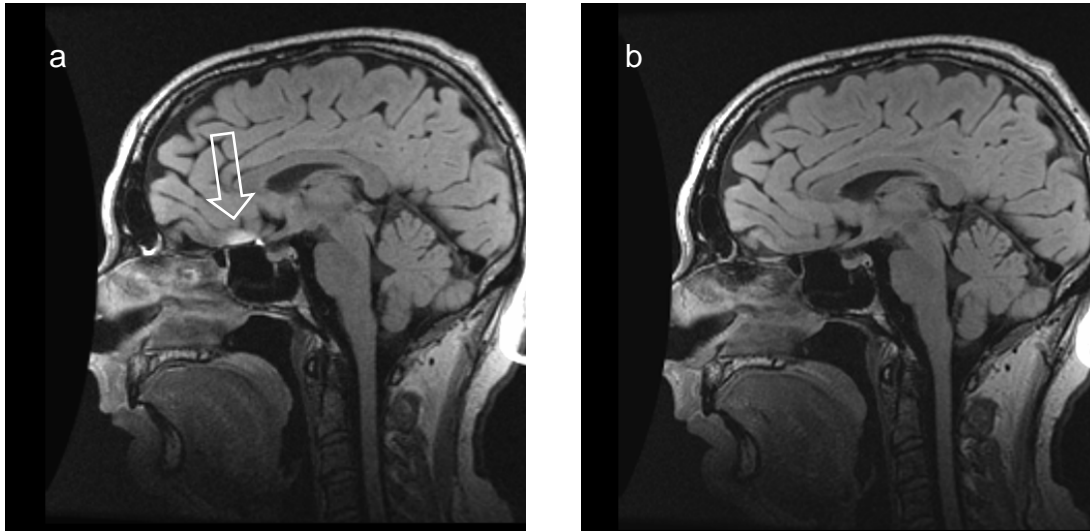
Figure 3. Sagittal 3D FLAIR image of a healthy volunteer at 3.0T. a) With an inversion RF bandwidth of 600 Hz, incomplete inversion in a region of rapid susceptibility variation causes a bright spot artifact (arrow). b) Increasing the RF inversion BW to 2000 Hz resolves the problem.
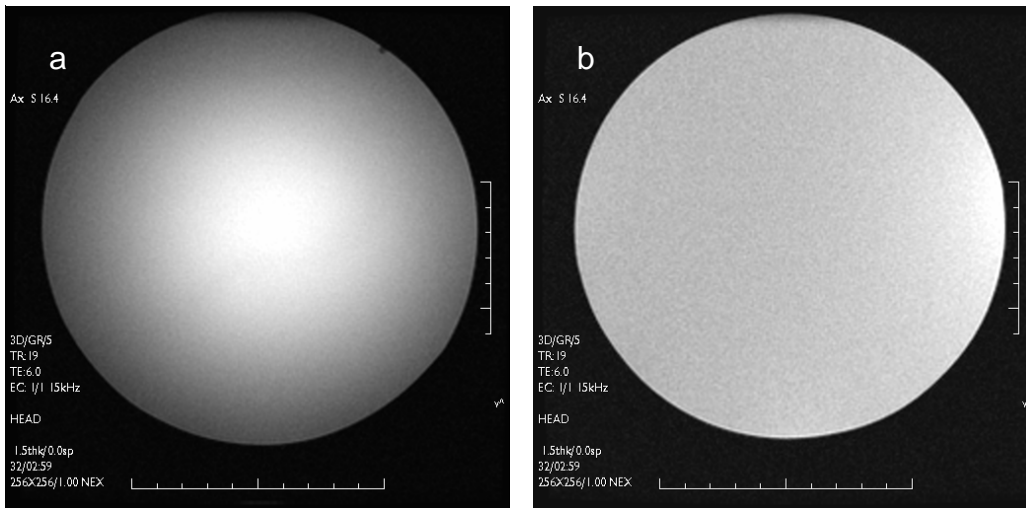

Figure 4. Images of spherical phantoms acquired with the same transmit/receive head coil, and imaging protocol. a) Image displaying dielectric resonance artifact (bright region in the center) with a water-based phantom. b) Oil-based phantom has more uniform image appearance. The intensity variations on (b) reflect the actual B1-sensitivity of the RF coil.

Acknowledgements